

ARTICLE TYPE

Euclidean Ideal Point Estimation From Roll-Call Data via Distance-Based Bipartite Network Models

Seungju Lee,[†] In Kyun Kim,^{†‡} Jong Hee Park,^{*‡} and Ick Hoon Jin^{*†}

[†]Department of Statistics and Data Science, Yonsei University, Republic of Korea.

[‡]Department of Political Science and International Relations, Seoul National University, Republic of Korea.

*Corresponding author. Email: jongheepark@snu.ac.kr; ijin@yonsei.ac.kr

Abstract

Conventional ideal point models rely on Gaussian or quadratic utility functions that violate the triangle inequality, producing non-metric distances that complicate geometric interpretation and undermine clustering and dispersion-based analyses. We introduce a distance-based alternative that adapts the Latent Space Item Response Model (LSIRM) to roll-call data, treating legislators and bills as nodes in a bipartite network jointly embedded in a Euclidean metric space. Through controlled simulations, Euclidean LSIRM consistently recovers latent coalition structure with superior cluster separation relative to existing methods. Applied to the 118th U.S. House, the model improves vote prediction and yields bill embeddings that clarify cross-cutting issue alignments. The results show that restoring metric structure to ideal point estimation provides a clearer and more coherent inference about party cohesion, factional divisions, and multidimensional legislative behavior.

Keywords: Legislative Voting, Ideal Point Estimation, Metric Spaces, Bipartite Networks, Coalition Structure

1. Introduction

Ideal point estimation from roll-call voting data has become a foundational tool in legislative studies, enabling systematic analysis of partisan polarization, ideological trajectories, and coalition dynamics (Poole and Rosenthal 2007; Clinton, Jackman, and Rivers 2004; McCarty 2016). The dominant methods—NOMINATE (Poole and Rosenthal 2007; Lewis et al. 2025) and Bayesian Item Response Theory (BIRT) (Clinton, Jackman, and Rivers 2004; Jackman 2024)—successfully recover ordinal ideological relationships and achieve high vote classification accuracy. Recent work expands these frameworks by incorporating domain-specific or multiple dimension (Moser, Rodríguez, and Lofland 2021; Marble and Tyler 2022; Binding and Stoetzer 2023; Lipman, Moser, and Rodriguez 2025), integrating text-based information (Kim, Londregan, and Ratkovic 2018), or accommodating both monotonic and non-monotonic response functions (Lei and Rodriguez 2025).

Yet despite these advances, existing models share a structural limitation: the utility functions underlying NOMINATE and BIRT do not induce proper metric distances. Their Gaussian and quadratic specifications violate the triangle inequality, the defining property of metric spaces. Although this issue is mathematically straightforward, its consequences for political analysis are substantive. When distances lack metric validity, dispersion statistics used to assess party cohesion become non-comparable, and clustering analyses may generate configurations in which A is “close” to B, B to C, yet A remains far from C. As contemporary legislatures exhibit growing intra-party heterogeneity (Clarke 2020; Harbridge-Yong, Volden, and Wiseman 2023), researchers increasingly rely on spatial distances to characterize factional structure, coalition tendencies, or ideological spread—applications for which non-metric utilities provide an unstable foundation.

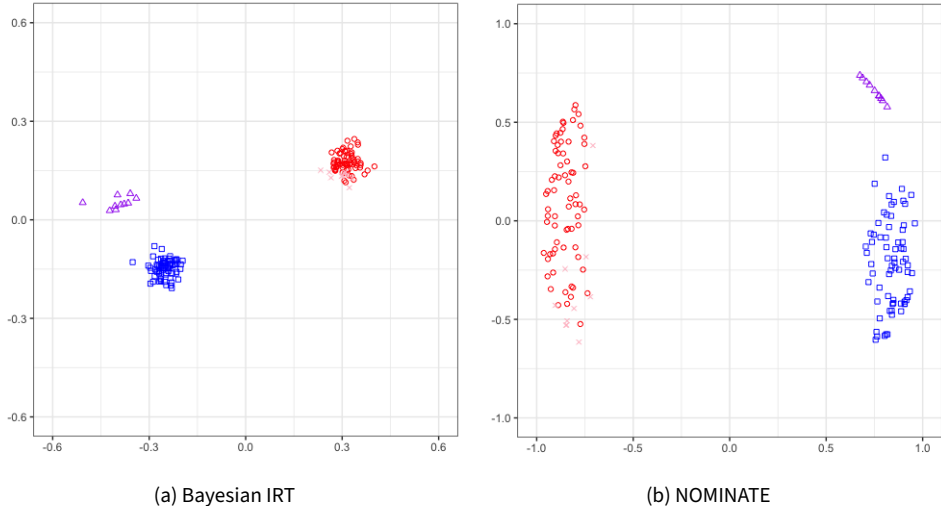


Figure 1. Coalition-cluster distortion in non-metric ideal point methods. Ground truth: **four distinct coalitions** (marked by colors and shapes)—Party A majority (70, blue squares) and minority (10, purple triangles); Party B majority (70, red circles) and minority (10, pink crosses). The 400-bill agenda includes 200 partisan bills (party-line division) and 200 faction-specific bills (50 per faction). Despite this clear structure, both BIRT (a) and NOMINATE (b) compress the four factions into approximately two party blocs, with faction markers overlapping substantially within parties.

The practical consequences are severe. Figure 1 demonstrates this problem through simulated data. We generated roll-call data for 160 legislators organized into four distinct coalitions. Specifically, we consider two parties (80–80), each of which split into a majority faction (70) and a minority faction (10). The legislative agenda comprised 200 partisan bills establishing party separation and 200 faction-specific bills (50 per faction) encoding within-party heterogeneity. Despite this transparent four-cluster structure, both NOMINATE and BIRT systematically compress factions into two party blocs. This is not estimation failure—both methods achieve high vote classification accuracy—but rather reflects the fundamental constraint that non-metric distances cannot support valid clustering analysis.

Recent work has recognized these limitations. Shin, Lim, and Park (2024) proposed an L_1 -norm model using Manhattan distance: $U(x, y) = -\sum_k w_k |x_k - y_k|$, which satisfies the triangle inequality and provides a valid metric. However, Manhattan distance creates interpretive difficulties for spatial visualization: the distance between two points depends on their axis-aligned path rather than the direct geometric separation, complicating intuitive understanding of ideological proximity.

In this paper, we propose using Euclidean distance (L_2 norm) $d(x, y) = \sqrt{\sum_k (x_k - y_k)^2}$, which provides both valid metric properties and intuitive geometric interpretability of spatial models. Euclidean distance satisfies the triangle inequality through the Cauchy–Schwarz inequality, provides the familiar notion of “straight-line” distance between points, and admits natural geometric interpretation of clusters as spatially coherent regions.

Our approach builds on the recent turn toward network-based measures of political ideology. Barberá (2015) develops a Bayesian spatial following model for Twitter data, where ideological proximity is inferred from follower networks. Although innovative, this approach relies on a quadratic distance formulation ($-\|x_i - x_j\|^2$), which violates the triangle inequality and thus inherits the same non-metric limitations as BIRT. Similar work by Lo, Olivella, and Imai (2023) treats cosponsorship as a bipartite network and estimates latent positions via a mixed-membership blockmodel, but the latent structure is categorical, and legislators and bills are represented through class membership rather than

geometric positions. In contrast to both approaches, we adopt the Latent Space Item Response Model (Jeon et al. 2021, LSIRM), which treats roll-call data explicitly as a bipartite legislator–bill network and embeds both node types jointly in a Euclidean metric space. This symmetric formulation enables bills to serve as interpretive anchors defining the meaning of latent dimensions, while Euclidean distance governs the voting probability through a monotone link. By adapting Euclidean LSIRM to legislative voting, we obtain ideal points that are geometrically interpretable, metric-consistent, and directly suitable for clustering and coalition analysis.

In the following, we provide theoretical and empirical evidence that non-metric utility functions systematically distort clustering inference: in controlled simulations with known four-coalition structures, NOMINATE and BIRT compress factions (silhouette coefficient: 0.778), while Euclidean LSIRM recovers the true structure (silhouette coefficient: 0.861). Second, we show that joint legislator–bill embedding enables substantive interpretation through bill locations as anchors: in the 118th House, war powers and surveillance bills position between Squad and Freedom Caucus members, clarifying cross-cutting cleavages that conventional methods obscure. Third, we demonstrate that Euclidean distance provides superior predictive performance (classification accuracy: 0.80 versus 0.72 for BIRT; APRE: 0.45 versus 0.23).

Section 2 establishes that conventional utility functions violate the triangle inequality and proves Euclidean distance provides a proper metric. Section 3 introduces the bipartite network framework and Euclidean LSIRM specification. Section 4 presents simulations demonstrating that metric properties enable correct cluster recovery. Section 5 applies the method to the 118th House, showing how bill embeddings serve as interpretive anchors for coalition structure. Section 6 concludes with implications and extensions.

2. Metric Properties of Utility Functions

2.1 Proximity Voting Theory and Metric Requirements

The theoretical foundation for spatial voting models rests on the proximity voting framework developed by Downs (1957) and formalized by Davis, Hinich, and Ordeshook (1970). Under this framework, each voter i possesses an ideal point x_i in a policy space, and evaluates alternatives by their distance from this ideal point. For a policy located at position y , the voter's utility follows:

$$U_i(y) = -d(x_i, y) + \epsilon_i, \quad (1)$$

where $d(\cdot, \cdot)$ represents a distance function and ϵ_i is a random utility component. The voter prefers alternative A over alternative B when $U_i(A) > U_i(B)$, which occurs when $d(x_i, A) < d(x_i, B)$ —that is, when A is closer to the voter's ideal point than B .

The proximity voting framework implicitly assumes that $d(\cdot, \cdot)$ constitutes a proper distance metric. Three properties are essential for the theoretical coherence of this framework. First, symmetry requires $d(x, y) = d(y, x)$: the ideological distance from position x to position y equals the distance from y to x . Without symmetry, the model would imply that moving from a liberal to conservative position involves a different ideological journey than moving from conservative to liberal, contradicting the reciprocal nature of ideological proximity. Second, the triangle inequality requires $d(x, y) + d(y, z) \geq d(x, z)$ for all points: the direct distance between two positions cannot exceed the sum of distances through an intermediate position. Without this property, indirect ideological paths could be shorter than direct paths, violating basic intuitions about ideological space and enabling paradoxical configurations where three positions cannot be consistently arranged along ideological dimensions. Third, positive definiteness requires $d(x, y) > 0$ for $x \neq y$ and $d(x, x) = 0$: distinct positions must be separated by positive distance, while a position's distance from itself is zero. Without this property, distinct ideological positions could be indistinguishable, rendering the spatial representation meaningless.

These metric properties are not merely mathematical conveniences—they are fundamental to the substantive interpretation of proximity voting. Consider the triangle inequality: if legislator A has ideal point close to position x , and position x is close to position y , the triangle inequality guarantees that legislator A cannot be arbitrarily distant from position y . This transitive consistency underlies claims about coalition formation: if moderate Democrats are close to centrist positions, and centrist positions are close to moderate Republicans, then moderate Democrats and moderate Republicans must be relatively proximate, enabling bipartisan coalitions. Without the triangle inequality, such transitive reasoning fails—proximity becomes intransitive, and the spatial metaphor loses coherent meaning.

In the following, we will show that conventional ideal point methods, despite being explicitly motivated by proximity voting theory, employ utility functions that violate these metric requirements.

2.2 The Triangle Inequality and Its Violation in Conventional Methods

A distance function $d : \mathcal{X} \times \mathcal{X} \rightarrow \mathbb{R}_+$ defines a metric space if it satisfies four properties: (1) non-negativity: $d(x, y) \geq 0$ with equality if and only if $x = y$; (2) symmetry: $d(x, y) = d(y, x)$; (3) triangle inequality: $d(x, y) + d(y, z) \geq d(x, z)$ for all $x, y, z \in \mathcal{X}$; and (4) identity of indiscernibles. The triangle inequality is particularly critical: it ensures that distances are additive, comparable, and transitively consistent. Without this property, distances lose cardinal meaning—we cannot meaningfully say one pair is “twice as distant” as another, compare separations across dimensions, or use distance-based clustering methods that assume metric structure.

Conventional ideal point methods employ utility functions that violate the triangle inequality. In BIRT (Clinton, Jackman, and Rivers 2004), legislators maximize quadratic utility derived from proximity voting: for each roll-call j presenting a binary choice between “Yea” position ζ_j and “Nay” position ψ_j , legislator i with ideal point x_i votes “Yea” when

$$-\|x_i - \zeta_j\|^2 + \eta_{ij} > -\|x_i - \psi_j\|^2 + \nu_{ij}.$$

Expanding and reparameterizing yields $P(y_{ij} = 1) = \Phi(\beta_j^\top x_i - \alpha_j)$ where $\beta_j = 2(\zeta_j - \psi_j)/\sigma_j$. However, this reparameterization induces a distance measure based on squared differences. Consider $d_Q(x, y) = (x - y)^2$ in one dimension. The triangle inequality requires $(x - y)^2 + (y - z)^2 \geq (x - z)^2$. Expanding $(x - z)^2 = [(x - y) + (y - z)]^2 = (x - y)^2 + 2(x - y)(y - z) + (y - z)^2$, the inequality reduces to $2(x - y)(y - z) \geq 0$. This fails whenever $(x - y)$ and $(y - z)$ have opposite signs.

In NOMINATE (Poole and Rosenthal 2007), legislators maximize Gaussian utility:

$$U_i(\zeta_j) = \beta \exp\left\{-\frac{1}{2} \sum_k w_k^2 (x_{ik} - \zeta_{jk})^2\right\}.$$

The exponential transformation of squared distances induces a non-metric similarity measure. Consider three points $x = 3$, $y = 3$, $z = 1$ in one dimension. Computing the Gaussian-based “distances”: $d_G(x, y) = -\exp\left\{-\frac{1}{2}(3 - 3)^2\right\} = -\exp\{0\} = -1$, $d_G(y, z) = -\exp\left\{-\frac{1}{2}(3 - 1)^2\right\} = -\exp\{-2\}$, $d_G(x, z) = -\exp\left\{-\frac{1}{2}(3 - 1)^2\right\} = -\exp\{-2\}$. The triangle inequality requires $d_G(x, y) + d_G(y, z) \geq d_G(x, z)$, or $-1 - \exp\{-2\} \geq -\exp\{-2\}$. This clearly fails. The exponential function is convex and destroys additivity: distances through intermediate points shrink dramatically relative to direct distances, violating the fundamental requirement that indirect paths cannot be shorter than direct paths.

These violations have direct consequences for legislative analysis. When researchers measure party cohesion as the standard deviation of ideal point estimates within a party, non-metric distances produce incomparable statistics: one party may appear more dispersed than another not because its members vote less cohesively, but because the non-metric utility function amplifies or compresses distances non-uniformly across the ideological space. This makes it impossible to meaningfully

compare party cohesion across parties, across time periods, or across different legislatures. When identifying factions through clustering algorithms applied to ideal point coordinates, which is done frequently in applied research, violations of the triangle inequality undermine the validity of cluster quality measures. Without metric properties, a faction appearing “cohesive” (small within-cluster distances) and “distinct” (large between-cluster distances) may reflect how the utility function distorts space rather than actual voting coalition structure. When comparing ideological conflict across policy dimensions (e.g., asking whether economic or social issues generate greater polarization), non-metric distances prevent meaningful statements about relative magnitudes because equal numerical separations on different dimensions may represent fundamentally different quantities. A two-unit difference on the first dimension may correspond to a substantively larger or smaller ideological gap than a two-unit difference on the second dimension, not because the dimensions capture different types of conflict, but because the non-metric utility function scales distances differently across regions of the space.

2.3 Euclidean Distance as a Metric

Euclidean distance $d_E(x, y) = \sqrt{\sum_{k=1}^K (x_k - y_k)^2}$ satisfies the triangle inequality and defines a proper metric space. The proof follows directly from the Cauchy-Schwarz inequality: for any three points $x, y, z \in \mathbb{R}^K$, squaring $d_E(x, y) + d_E(y, z) \geq d_E(x, z)$ and expanding yields $d_E(x, y)d_E(y, z) \geq \sum_k (x_k - y_k)(y_k - z_k)$, which holds because $|\sum_k (x_k - y_k)(y_k - z_k)| \leq \sqrt{\sum_k (x_k - y_k)^2} \sqrt{\sum_k (y_k - z_k)^2} = d_E(x, y)d_E(y, z)$ by Cauchy-Schwarz.

This metric property has direct implications for legislative analysis. First, distances become cardinally interpretable: if $d_E(z_A, z_B) = 2d_E(z_C, z_D)$, legislators *A* and *B* are genuinely twice as ideologically separated as *C* and *D* in their voting behavior. Second, distances become comparable across dimensions: we can meaningfully ask whether the first or second dimension generates greater polarization by comparing distance statistics, because the metric structure ensures these comparisons reflect substantive differences rather than measurement artifacts. Third, clustering methods that assume metric distances—*k*-means, hierarchical clustering, silhouette analysis—produce valid results rather than artifacts of non-metric geometry. For example, the silhouette coefficient, which measures cluster quality through the ratio of within-cluster to between-cluster distances, requires the triangle inequality to ensure that clusters represent genuine spatial coherence rather than projection artifacts. Fourth, the geometric interpretation aligns with mathematical properties: points that appear close in two-dimensional visualizations genuinely vote similarly, and spatial neighborhoods correspond to actual voting coalitions rather than distortions induced by non-metric utility functions.

3. Euclidean Distance Model for Bipartite Legislative Networks

3.1 Bipartite Network Framework

Roll-call voting data constitute a bipartite network linking legislators to bills through binary votes (excluding abstention). Conventional ideal point methods treat this structure asymmetrically: legislators receive interpretable spatial positions (ideal points) while bills serve merely as instruments for scaling, with bill parameters (α_j, β_j) estimated but not embedded in the same space. The reparameterization from spatial bill positions (ζ_j, ψ_j) to discrimination parameters (α_j, β_j) is many-to-one—entirely different bill locations generate identical parameters—making bills uninterpretable as spatial entities (Shin, Lim, and Park 2024; Nakis et al. 2025).

Instead, we treat roll-call voting as a bipartite network where both legislators and bills occupy interpretable positions in a shared metric space. This symmetric treatment enables three types of analysis: legislator-to-legislator distances reveal ideological similarities, bill-to-bill distances identify policy clustering, and legislator-bill distances clarify which coalitions support which bills.

Following Hoff, Raftery, and Handcock (2002) and Hoff (2007), we model the voting relationship through latent space embeddings. For legislator i with latent position $z_i \in \mathbb{R}^K$ and bill j with latent position $w_j \in \mathbb{R}^K$, the probability of a “Yea” vote depends on their spatial relationship:

$$g(\Pr(y_{ij} = 1 | z_i, w_j)) = \mu + \alpha(z_i, w_j), \quad (2)$$

where $g(\cdot)$ denotes a link function and $\alpha(z_i, w_j)$ specifies how latent positions determine voting propensity. Three canonical specifications exist. The latent class model (LCM, Holland, Laskey, and Leinhardt 1983; Nowicki and Snijders 2001; Airolди et al. 2008; Miller, Jordan, and Griffiths 2009; Mørup, Schmidt, and Hansen 2011; Palla, Knowles, and Ghahramani 2012; Zhou 2015) and stochastic blockmodel (SBM, Holland, Laskey, and Leinhardt 1983; Nowicki and Snijders 2001; Airolди et al. 2008; Daudin, Picard, and Robin 2008; Karrer and Newman 2011; Vu, Hunter, and Schweinberger 2013)) sets $\alpha(z_i, w_j) = m_{u_i, v_j}$ for discrete group memberships $u_i, v_j \in \{1, \dots, K\}$ and interaction matrix $M = (m_{k\ell})$, capturing stochastic equivalence where legislators in the same class vote identically. The latent eigenmodel (Hoff 2007; Young and Scheinerman 2007; Hoff 2009; Li, Yeung, and Zhang 2011; Hoff 2021) defines $\alpha(z_i, w_j) = z_i^\top \Lambda w_j$ for diagonal matrix Λ , representing voting through weighted inner products that extend principal component analysis to binary data. The latent distance model (Hoff, Raftery, and Handcock 2002; Schweinberger and Snijders 2003; Kemp et al. 2006; Handcock, Raftery, and Tantrum 2007; Hoff 2007; Krivitsky and Handcock 2008; Raftery et al. 2012; Sewell and Chen 2015; Smith, Asta, and Calder 2019) specifies $\alpha(z_i, w_j) = -\gamma \|z_i - w_j\|$, where voting probability decreases monotonically with spatial separation, operationalizing homophily through spatial proximity.

Distance-based specifications have been applied to political networks in two contexts, though with different formulations and objectives than ours. Barberá (2015) employed a latent space model to estimate ideal points from Twitter following patterns, treating the data as a bipartite network where users choose whether to follow political actors. Users i and political actors j are embedded in a shared latent space, with following probability modeled as $P(y_{ij} = 1) = f(\phi - \gamma \|\theta_i - \beta_j\|^2)$, where $\|\theta_i - \beta_j\|^2$ represents squared Euclidean distance. However, this squared distance formulation—identical to BIRT’s quadratic utility—violates the triangle inequality and produces non-metric estimates with the same fundamental limitations we identify for conventional ideal point methods. Jeon et al. (2021) introduced the Latent Space Item Response Model (LSIRM) for educational testing, demonstrating how joint embedding of examinees and test items using Euclidean distance reveals item-respondent interaction patterns invisible to traditional IRT models. While the mathematical formulation is similar to what we employ, Jeon et al. (2021)’s application emphasizes psychometric properties—identifying which items differentiate ability levels and detecting unexpected response patterns—rather than the metric structure required for clustering and coalition analysis in legislative contexts.

Our contribution lies in recognizing that the choice between squared distance $\|\cdot\|^2$ and Euclidean distance $\|\cdot\|$ is not merely a modeling preference but fundamentally determines whether estimates support distance-based inference. By adapting LSIRM’s Euclidean specification to legislative voting with explicit attention to metric properties, we demonstrate that bill embeddings serve as interpretive anchors that define the substantive meaning of latent dimensions and enable valid identification of coalition structure—advantages unavailable when either (1) bills are treated merely as scaling instruments with uninterpretable parameters, or (2) distances are squared and thus non-metric.

3.2 Euclidean Distance Specification

We specify voting probability through Euclidean distance in a bipartite network framework. For legislator i with latent position $z_i \in \mathbb{R}^K$ and bill j with latent position $w_j \in \mathbb{R}^K$:

$$\text{logit}(P(y_{ij} = 1 | \theta_i, \beta_j, \gamma, z_i, w_j)) = \theta_i + \beta_j - \gamma \|z_i - w_j\|, \quad (3)$$

where θ_i captures legislator i 's baseline propensity to vote "Yea", β_j represents bill j 's baseline popularity or controversy, and $\gamma > 0$ governs the strength of proximity effects. The Euclidean distance is $\|z_i - w_j\| = \sqrt{\sum_{k=1}^K (z_{ik} - w_{jk})^2}$. The probability of a "Yea" vote increases with legislator propensity θ_i and bill popularity β_j , but decreases with spatial distance $\|z_i - w_j\|$. This formulation directly implements proximity voting (Downs 1957; Davis, Hinich, and Ordeshook 1970): legislators support bills near their ideal points, with support declining monotonically as separation increases.

The baseline parameters θ_i and β_j play distinct roles from conventional IRT. In BIRT, the intercept α_j conflates bill location and difficulty because it equals $(\zeta_j^\top \zeta_j - \psi_j^\top \psi_j)/\sigma_j$, mixing spatial position with variance scaling. In our specification, β_j measures only the baseline tendency for legislators to support bill j averaging over all spatial locations—a pure "how popular is this bill" parameter separable from its ideological location w_j . Similarly, θ_i measures legislator i 's general tendency to vote "Yea" independent of ideological proximity—some legislators vote "Yea" frequently (high θ_i) while others vote "Nay" frequently (low θ_i) for reasons orthogonal to spatial positioning. This separation between baseline propensities and spatial structure, which is similar to the degree correction in network science literature (Fortunato 2010), clarifies interpretation: if legislator i supports bill j , we can determine whether this reflects high baseline propensity (θ_i or β_j large), ideological proximity ($\|z_i - w_j\|$ small), or both.

The parameter γ quantifies the strength of spatial proximity relative to baseline propensities. Large γ indicates voting is primarily distance-determined—legislators vote almost exclusively for nearby bills regardless of baseline propensities—while small γ suggests the dominance of baseline propensities, a spatial structure playing a secondary role. This provides diagnostic information about legislative organization: chambers with strong, stable party or factional discipline exhibit larger γ (tight clustering with sharp spatial boundaries), whereas fragmented or weakly organized chambers exhibit smaller γ (diffuse positioning where baseline propensities matter more than ideological location). Our simulation studies demonstrate that γ responds predictably to known levels of coalition cohesion, increasing when within-group homogeneity strengthens and decreasing when independent voting attenuates the distance signal.

The bipartite embedding provides three interpretive advantages over conventional methods. First, legislator-to-legislator distances $\|z_i - z_{i'}\|$ reveal ideological similarities based on voting patterns, enabling valid clustering analysis because Euclidean distance satisfies the triangle inequality. Second, bill-to-bill distances $\|w_j - w_{j'}\|$ identify policy clustering—bills with similar coalitions locate proximately, revealing which issues align and which cross-cut party lines. Third, direct legislator-bill distances $\|z_i - w_j\|$ clarify coalition structure through spatial proximity: partisan bills cluster near their party's centroid, faction-specific bills appear as satellites adjacent to target factions, and cross-party "bridge" bills position between cooperating legislators from different parties. This joint embedding enables interpretation through bill locations as anchors: instead of asking "what does dimension 2 mean?", we can observe "which bills define dimension 2?" and infer substantive meaning from the specific legislation that separates high from low values.

3.3 Full Conditionals and Estimation

We estimate parameters via Markov Chain Monte Carlo (MCMC) sampling with the Gibbs sampling and the metropolis-Hastings algorithm with the following prior specifications:

$$\begin{aligned}
\theta_i &\sim N(0, \sigma_\theta^2), \\
\beta_j &\sim N(0, \sigma_\beta^2), \\
\sigma_\theta^2 &\sim \text{Inv-Gamma}(a_\sigma, b_\sigma), \\
z_i &\sim \text{MVN}_K(\mathbf{0}, \mathbf{I}_K), \\
w_j &\sim \text{MVN}_k(\mathbf{0}, \mathbf{I}_k), \\
\log \gamma &\sim N(\mu_\gamma, \sigma_\gamma^2).
\end{aligned} \tag{4}$$

Then, the joint posterior density of the model is given as

$$\begin{aligned}
\pi(\beta, \theta, \gamma, \mathbf{Z}, \mathbf{W} \mid \mathbf{Y}) &\propto \prod_{i=1}^N \prod_{j=1}^P P(Y_{ij} = \gamma_{ij} \mid \theta_i, \beta_j, \gamma, z_i, w_j) \\
&\times \pi(\gamma) \prod_{j=1}^P \pi(\beta_j) \prod_{i=1}^N \pi(\theta_i) \prod_{i=1}^N \pi(z_i) \prod_{j=1}^P \pi(w_j)
\end{aligned} \tag{5}$$

The priors and the following posterior distribution can be expressed in equations 4 and 5. This posterior kernel cannot be expressed with standard distribution, so the exact posterior density cannot be calculated and a Gibbs sampler is used to sample each parameter sequentially from their conditional density. Specifically, because each conditional kernel may not be expressed as a standard distribution form, Metropolis-Hastings within Gibbs sampler is used. Furthermore, for the generalized case with missing data, the imputed value for the non-respondent pair can be sampled with the logistic formula at the start of each Gibbs sampler step.

$$\begin{aligned}
\pi(\theta_i) &\propto \left[\prod_{i=1}^N \prod_{j=1}^P P(Y_{ij} = \gamma_{ij} \mid \theta_i, \beta_j, \gamma, z_i, w_j) \right] \times [N_{\theta_i}(0, \sigma_\theta^2)] \\
\pi(\beta_j) &\propto \left[\prod_{i=1}^N \prod_{j=1}^P P(Y_{ij} = \gamma_{ij} \mid \theta_i, \beta_j, \gamma, z_i, w_j) \right] \times [N_{\beta_j}(0, \sigma_\beta^2)] \\
\pi(\log \gamma) &\propto \left[\prod_{i=1}^N \prod_{j=1}^P P(Y_{ij} = \gamma_{ij} \mid \theta_i, \beta_j, \gamma, z_i, w_j) \right] \times [N(\mu_\gamma, \sigma_\gamma^2)] \\
\pi(z_i) &\propto \left[\prod_{i=1}^N \prod_{j=1}^P P(Y_{ij} = \gamma_{ij} \mid \theta_i, \beta_j, \gamma, z_i, w_j) \right] \times [\text{MVN}_{K, z_i}(\mathbf{0}, \mathbf{I}_K)] \\
\pi(w_j) &\propto \left[\prod_{i=1}^N \prod_{j=1}^P P(Y_{ij} = \gamma_{ij} \mid \theta_i, \beta_j, \gamma, z_i, w_j) \right] \times [\text{MVN}_{K, w_j}(\mathbf{0}, \mathbf{I}_k)] \\
\pi(\sigma_\theta) &\propto \text{Inv-Gamma} \left(\left(\frac{N}{2} + a_\sigma \right), \frac{1}{2} \sum_{i=1}^N \theta_i^2 + b_\sigma \right)
\end{aligned}$$

Like conventional ideal-point estimators, Euclidean LSIRM inherits rotational, reflective, and translational indeterminacies: for any orthogonal matrix Q and vector c , the transformed configuration

$(Qz_i + c, Qw_j + c)$ produces identical probabilities. Because we do not fix the positions of any legislators or bills, the absolute orientation and location of the latent space are not identified. We identify the configuration through post-processing alignment to principal axes.

4. Simulation Studies

We designed three simulations to evaluate Euclidean LSIRM against BIRT under conditions that progressively increase in complexity. Each simulation addresses a specific question:

1. Cohesion Gradient: Does the proximity parameter γ respond appropriately to known levels of group cohesion?
2. Cluster Recovery: Can the model recover multiple independent clusters in low-dimensional space?
3. Party–Faction Structure: Can the model distinguish factions within parties and cross-party coalitions?

All simulations used 100 replicated datasets. MCMC chains ran for 30,000 iterations with 5,000 burn-in and thinning factor 5. We evaluate performance using the estimated proximity strength $\hat{\gamma}$, silhouette coefficients, and visual inspection of latent embeddings.

4.1 Simulation 1: Cohesion Gradient

We created a legislature with 100 legislators organized into 10 groups (5 per bloc), voting on 52 bills that pit the two blocs against each other. We manipulated cohesion by varying the proportion of *independent voters* within each group—legislators who vote “Yea” with probability p rather than following their bloc. As the independent proportion increases from 0% to 50%, group cohesion degrades. If γ captures proximity-based voting, higher independence should yield lower $\hat{\gamma}$. Additional variants of this cohesion gradient design, including all-bloc-combination and fully homogeneous two-bloc scenarios, are presented in the supplementary material.

Table 1. Estimated proximity strength $\hat{\gamma}$ (mean and SD) across 100 replications. Columns vary the percentage of independent voters; rows vary their “Yea” probability p .

		Independent Voter Proportion					
		10%	20%	30%	40%	50%	
p		0.50	3.633 (0.271)	2.288 (0.273)	1.513 (0.070)	1.211 (0.020)	0.992 (0.017)
		0.70	3.704 (0.052)	2.696 (0.034)	2.149 (0.028)	1.770 (0.024)	1.464 (0.023)

Table 1 supports this prediction. When independent voters behave randomly ($p = 0.5$), $\hat{\gamma}$ declines steeply from 3.63 to 0.99 as independence rises. When they lean toward “Yea” ($p = 0.7$), degradation is slower because the reduced binomial variance— $p(1 - p)$ is lower at 0.7 than at 0.5—preserves more within-bloc co-voting. The corresponding latent maps (Figure 2) show that at low independence, subgroups within each bloc cluster tightly; at high independence, boundaries blur. The γ parameter thus serves as a reliable index of distance-based voting strength.

4.2 Simulation 2: Cluster Recovery

We created $K \in \{5, 6\}$ disjoint clusters of 20 legislators each, with each cluster supporting a unique set of 100 bills. Targeted clusters vote “Yea” with probability p ; non-targeted clusters vote “Yea” with probability q . We varied signal strength using $(p, q) \in \{(0.90, 0.10), (0.80, 0.20), (0.70, 0.30)\}$. Euclidean LSIRM should recover all K clusters as compact, well-separated groups. BIRT, lacking metric structure, may collapse clusters along dominant axes.

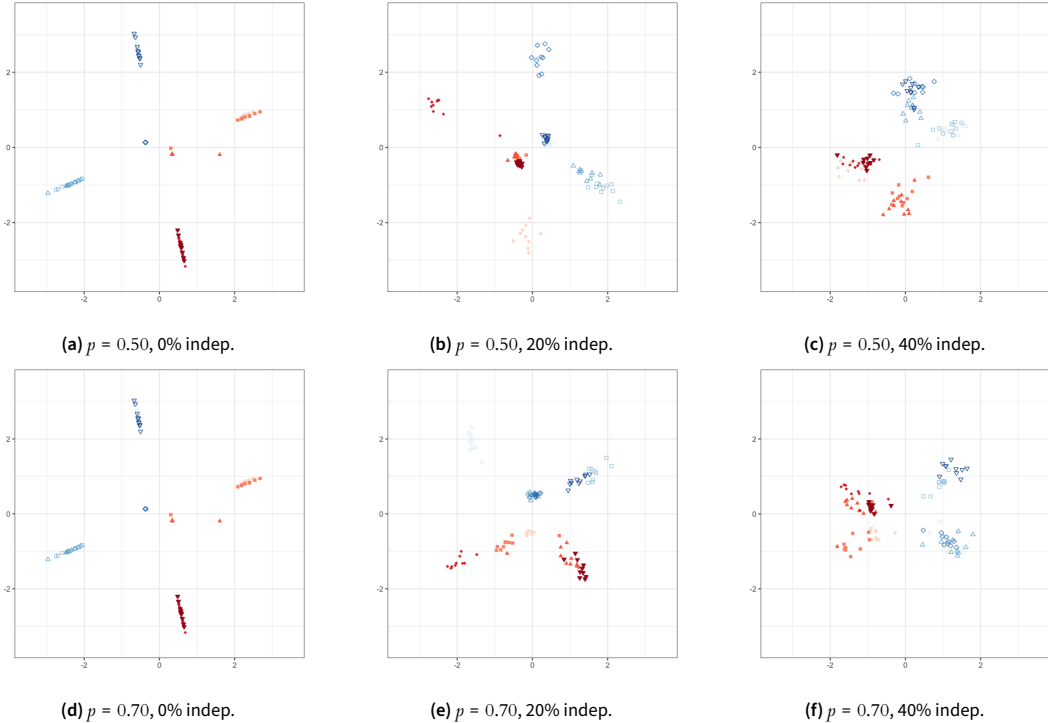


Figure 2. Euclidean LSIRM latent positions for Simulation 1. Each panel shows ideal point estimates for 10 legislative groups organized into two blocs (red filled markers vs. blue open markers). Columns vary independent voter proportion; rows vary “Yea” probability p .

Figure 3 presents results for the moderate-noise condition $(p, q) = (0.80, 0.20)$. Euclidean LSIRM produces compact, well-separated clusters with high silhouette scores ($M = 0.861$, $SD = 0.009$ for $K = 5$). BIRT partially collapses multiple clusters into elongated bands with significant overlap, yielding lower and more variable silhouettes ($M = 0.778$, $SD = 0.032$). The performance gap widens as K increases from 5 to 6, demonstrating that non-metric distances increasingly distort clustering inference as structural complexity grows. Analyses for the high- and low-signal regimes $(0.90, 0.10)$ and $(0.70, 0.30)$ with $K = 5$ and $K = 6$, as well as all three signal levels $(0.90, 0.10)$, $(0.80, 0.20)$, and $(0.70, 0.30)$ for $K = 4$, are presented in the supplementary material.

4.3 Simulation 3: Party–Faction Structure

This simulation tests performance under realistic conditions: two parties with internal factions, plus cross-party coalitions. The baseline structure consists of two parties, each containing two or three factions. We generated three types of bills: *partisan bills* supported by one party against the other, *faction bills* supported by a single faction, and *bridge bills* supported by factions from opposing parties. We examined three scenarios:

4.3.1 Agenda Sweep

Each party contains three factions (180 legislators total). We varied the share of partisan bills from 30% to 50%, with the remainder being faction-specific bills.

With 50% partisan bills, Euclidean LSIRM recovers all six factions as distinct clusters; BIRT collapses factions within parties (Figure 4). Reducing partisan bills to 30% amplifies faction signals—LSIRM improves further while BIRT remains locked onto the party axis.

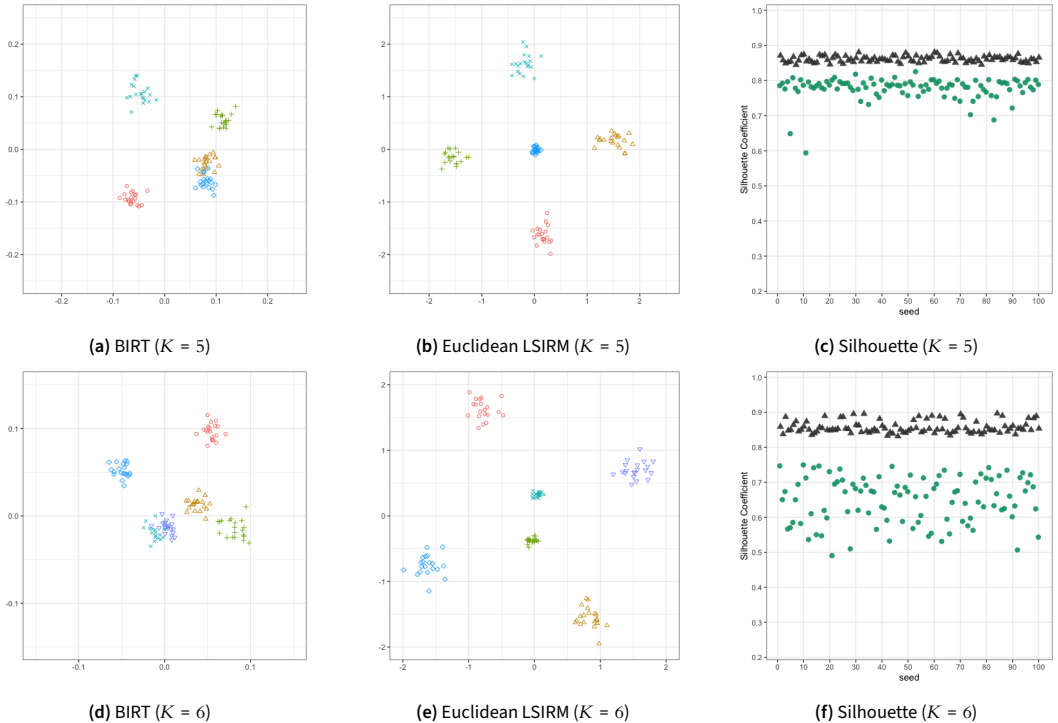


Figure 3. Cluster recovery under moderate noise ($p = 0.80, q = 0.20$). Left and center columns show representative latent maps; colors denote ground-truth cluster membership. Right column shows silhouette distributions over 100 replications (Euclidean LSIRM: black triangles; BIRT: green circles).

4.3.2 Noise Sweep

Each party contains two factions (80 legislators total). We fixed the agenda and varied voting noise: targeted factions support their bills with probability $p = 0.95$, while non-targeted factions support with probability $q \in \{0.10, 0.20\}$. Further analyses exploring a broader range of noise levels and alternative (p, q) settings appear in the supplementary material.

At low noise ($q = 0.10$), both models visually separate factions, but Euclidean LSIRM produces more compact clusters (Figure 5). At higher noise ($q = 0.20$), BIRT begins merging factions into party centroids while LSIRM remains robust. The LSIRM embedding also reveals interpretable bill behavior: faction-specific bills drift inward as their signal weakens.

Table 2. Overview of Simulation 3 scenarios.

Scenario	Manipulation	Key Test
(i) Agenda Sweep	Vary partisan vs. faction bill ratio	Faction recovery as partisan signal weakens
(ii) Noise Sweep	Vary voting noise (p, q)	Robustness of faction recovery
(iii) Cross-Party Coalitions	Add bridge bills	Representation of overlapping coalitions

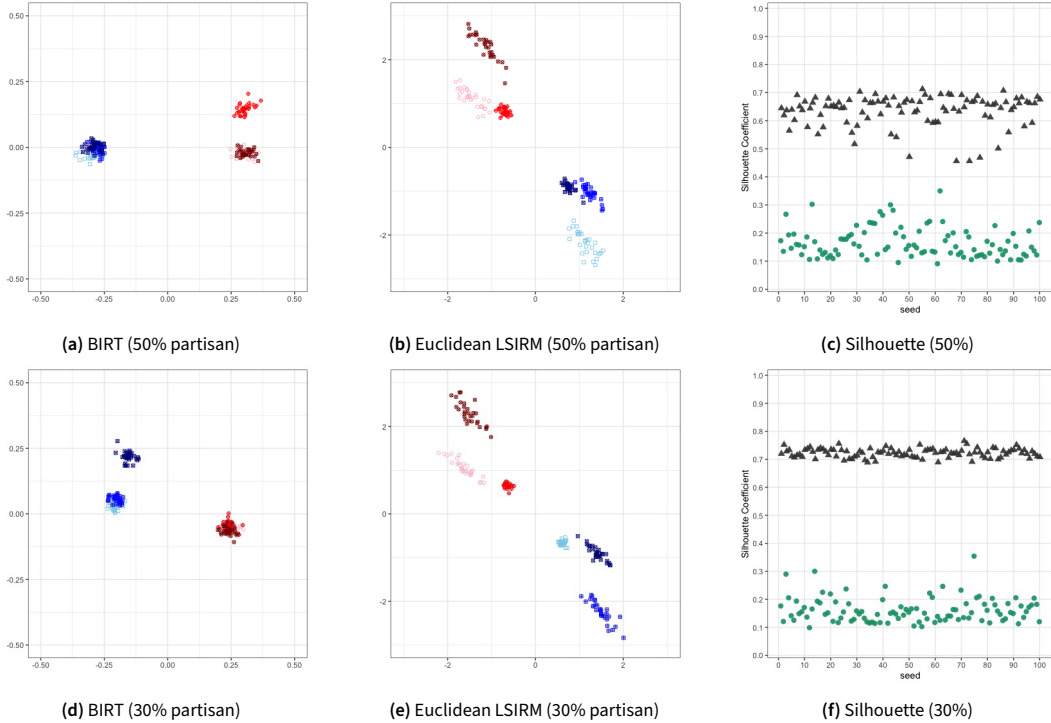


Figure 4. Fraction recovery under shifting legislative agendas. Colors and markers denote six true factions. Silhouette distributions: Euclidean LSIRM (black triangles), BIRT (green circles).

4.3.3 Cross-Party Coalitions

We introduced unequal fraction sizes (70 vs. 10 legislators per faction) and two types of bridge bills: *Bridge-A* supported by majority factions from both parties (L1 and C1), and *Bridge-B* supported by minority factions (L2 and C2). This design tests whether the model can represent overlapping coalitions that transcend party lines. Additional configurations and extended results, including simulations incorporating fraction bills, appear in the supplementary material.

In the majority consensus scenario (Figure 6), Euclidean LSIRM correctly draws the allied majority factions closer together near the inter-party boundary, with *Bridge-A* bills positioned between them ($\hat{\gamma} \approx 3.178$). BIRT fails to represent this structure—distances between allied cross-party legislators are no shorter than distances between ideological opponents.

In the ends-against-the-middle scenario (Duck-Mayr and Montgomery 2023a), Euclidean LSIRM draws the minority factions toward each other while maintaining separation between the majority blocs (Figure 7, $\hat{\gamma} \approx 3.206$). BIRT spreads legislators along a secondary axis in ways that obscure the coalition logic.

4.4 Simulation Summary

Across all three simulations, Euclidean LSIRM consistently outperforms BIRT in recovering known latent structures. The key advantages stem from the metric properties of Euclidean distance: the triangle inequality ensures that proximity corresponds meaningfully to voting similarity, enabling the model to represent multiple clusters, factions within parties, and cross-party coalitions. The proximity parameter γ provides an interpretable index of distance-based voting strength. These properties make Euclidean LSIRM well-suited for analyzing legislatures with complex coalition

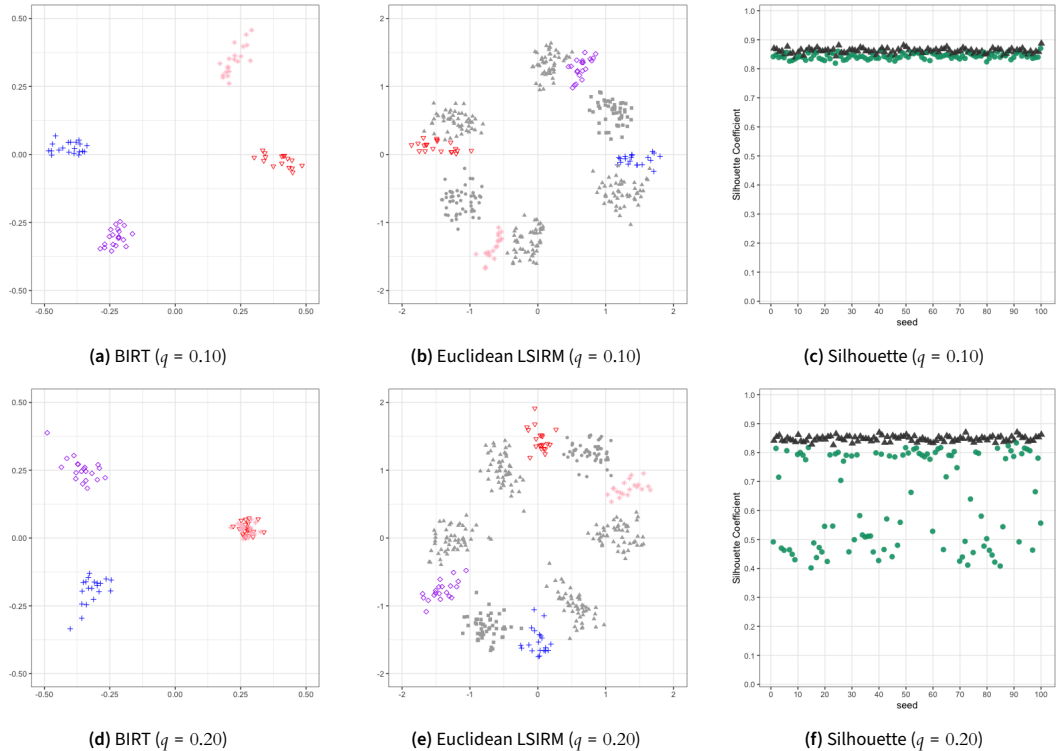


Figure 5. Fraction recovery under varying noise levels. Euclidean LSIRM maps include bill positions (gray markers). Silhouette distributions: Euclidean LSIRM (black triangles), BIRT (green circles).

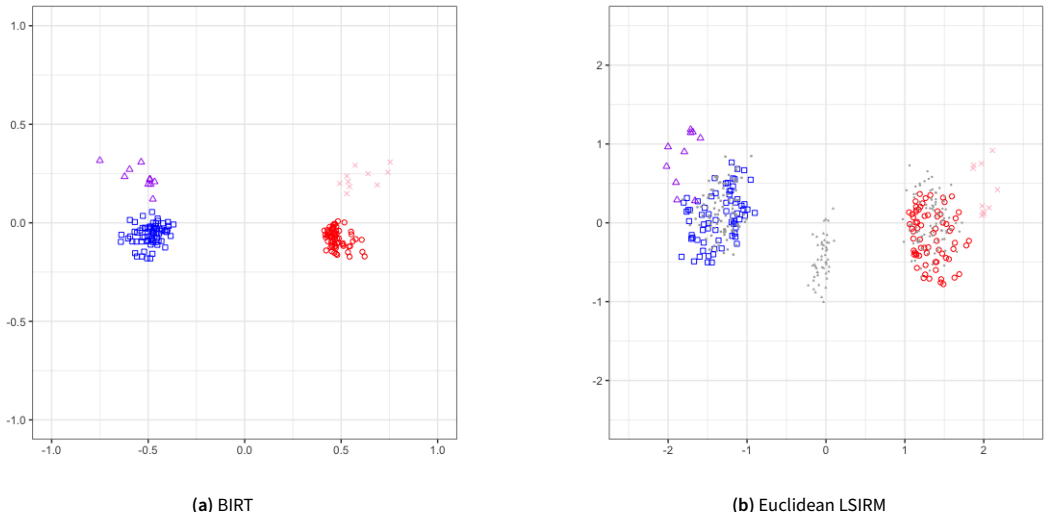


Figure 6. Majority consensus scenario. Legislators colored by party; shaped by faction (L1: blue squares, L2: purple triangles, C1: red circles, C2: pink crosses). Euclidean LSIRM draws allied majority fractions (L1, C1) closer together, with Bridge-A bills (grey triangle) positioned between them.

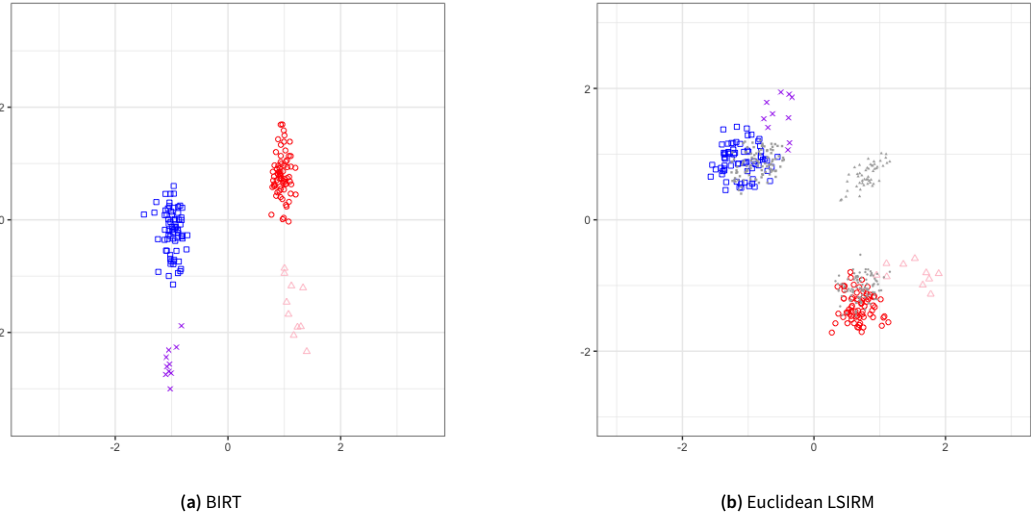


Figure 7. Ends-against-the-middle scenario. Euclidean LSIRM draws minority factions (L2, C2) toward each other, with Bridge-B bills (grey triangle) near this pairing.

structures.

5. Application: 118th U.S. House of Representatives

5.1 Data and Context

We apply Euclidean LSIRM to roll-call votes from the 118th U.S. House, obtained from Voteview (Lewis *et al.* 2025). Following standard practice, we excluded lopsided votes (overwhelming majorities) that provide little ideological information, yielding 1,225 informative roll-calls across 451 unique legislators (accounting for vacancies and replacements). This chamber provides a stringent test: extreme partisan polarization (the most conservative Democrat remains left of the most moderate Republican) yet well-documented intra-party factions—the progressive “Squad” (approximately 8 members) among Democrats and the House Freedom Caucus (approximately 22 members) among Republicans. These factions, though numerically small, exert disproportionate influence on leadership contests and agenda setting, making their accurate identification substantively important. The question is whether metric properties enable differentiation of these factions where non-metric methods collapse them into party blobs. MCMC diagnostics (trace plots for γ , bill positions, and legislator positions) in the supplementary material show well-mixed, stationary chains, confirming that the posterior embeddings analyzed below are based on converged samples.

5.2 Legislator Positions and Faction Recovery

Figure 8 displays two-dimensional embeddings from Euclidean LSIRM and BIRT. Both methods recover clear party separation on the primary (horizontal) dimension, with Democrats left and Republicans right. However, the secondary dimension reveals striking differences. Euclidean LSIRM differentiates factions: Freedom Caucus members (e.g., Andy Biggs, Paul Gosar) occupy far-right positions with distinctly negative second-dimension coordinates, separating them from mainstream Republicans, while Squad members (e.g., Ilhan Omar, Alexandria Ocasio-Cortez) appear below with slightly negative values, distinguishing them from other Democrats. The second dimension has substantial variance ($SD = 0.74$) in Euclidean LSIRM, indicating genuine factional structure. BIRT places faction members simply at extremes of the left-right continuum without meaningful

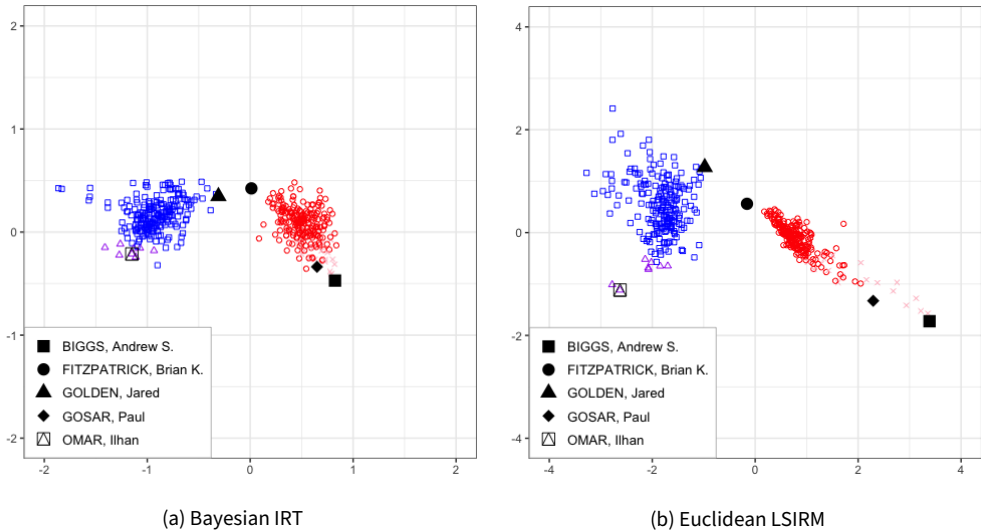


Figure 8. Two-dimensional ideal point estimates for the 118th U.S. House. Legislators are plotted by party and factional affiliation: Mainstream Democrats (blue squares), “Squad” Democrats (purple triangles), Mainstream Republicans (red circles), and Freedom Caucus Republicans (pink crosses).

secondary differentiation (SD of dimension 2 = 0.18 versus 0.74 for dimension 1), effectively collapsing multi-dimensional coalition structure into one-dimensional ordering.

Quantitatively, Euclidean LSIRM achieves superior performance on multiple metrics. Classification accuracy reaches 0.80 for Euclidean LSIRM versus 0.72 for BIRT, indicating the Euclidean embedding better predicts individual votes. The Aggregate Proportional Reduction in Error (APRE), which accounts for vote margins by comparing errors to baseline minority-vote predictions, reaches 0.45 for Euclidean LSIRM versus 0.23 for BIRT, demonstrating improvement particularly for close votes where clustering structure matters most. These gains reflect not merely better fit but more faithful representation of the underlying coalition structure: metric distances enable the model to differentiate factions spatially rather than compressing them along a single non-metric dimension.

5.3 Bill Embeddings as Interpretive Anchors

A key advantage of the bipartite network approach is that bill locations serve as interpretive anchors clarifying the substantive meaning of latent dimensions. Figure 9 displays the full legislator-bill embedding. Partisan bills cluster near their respective party centroids: Republican-supported bills (e.g., tax cuts, defense spending) locate in the far-right region near mainstream Republicans, while Democratic-supported bills (e.g., social programs, environmental regulation) cluster in the left region near mainstream Democrats. This validates that the first dimension captures the familiar liberal-conservative divide.

More revealing are bills that deviate from party centroids. War powers resolutions H.Con.Res. 21 (Syria withdrawal), H.Con.Res. 30 (Somalia withdrawal) and H.J.Res. 79 (terminating national emergency) position in the lower-left quadrant between Squad and Freedom Caucus locations (coordinates approximately $x \approx -0.5$, $y \approx -2$). These resolutions received support primarily from these two factions—progressive Democrats and libertarian Republicans—while being opposed by party establishments. Similarly, surveillance and privacy bills including H.R. 4755 (Privacy Enhancing Technology Research Act), H.R. 5403 (CBDC Anti-Surveillance State Act) locate far from the two extremist factions. These bill positions clarify the substantive meaning of the second dimension: it captures an establishment-outsider cleavage where ideological extremes from both parties converge

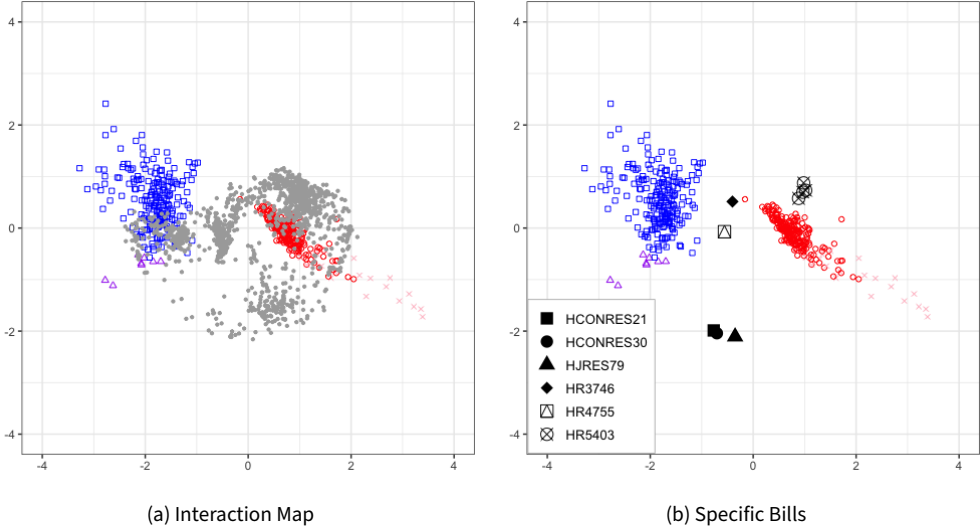


Figure 9. Two-dimensional ideal point estimates for the 118th U.S. House. Legislators are plotted by party and factional affiliation: Mainstream Democrats (blue squares), “Squad” Democrats (purple triangles), Mainstream Republicans (red circles), and Freedom Caucus Republicans (pink crosses). Bills are represented by gray markers.

against centrists on issues of foreign military intervention and government surveillance—the “horse-shoe” pattern where far-left and far-right align against the center (Duck-Mayr and Montgomery 2023b).

The debt-limit deal H.R. 3746 positions near the center in LSIRM’s embedding ($x \approx -0.4$, $y \approx 0.5$), reflecting its passage through a Democratic-anchored coalition with substantial Republican support—a bipartisan compromise occupying ideological middle ground. In contrast, BIRT cannot provide this interpretation because bills are not embedded spatially. The discrimination parameter β_j measures directional alignment but does not locate bills in the ideological space, precluding direct visualization of which bills define which dimensions. Without bill embeddings, conventional methods cannot directly show where such compromise legislation locates relative to partisan bills and extremist-coalition bills, obscuring the multi-dimensional coalition structure that characterizes contemporary congressional politics. Additional analyses in the supplementary material visualize bill locations together with within-faction Yea ratios, providing a finer-grained view of how factional support patterns align with Euclidean LSIRM’s spatial geometry.

6. Discussions

Conventional ideal point estimation methods employ utility functions that violate the triangle inequality, preventing meaningful interpretation of distance magnitudes and ratios. This non-metric structure systematically distorts clustering inference: in controlled simulations with known four-coalition structures, NOMINATE and BIRT compress factions into party blobs (silhouette coefficients: 0.778), while Euclidean LSIRM recovers the true structure (0.861). Application to the 118th House demonstrates how metric properties enable substantive interpretation: bill embeddings position war powers and surveillance legislation between Squad and Freedom Caucus members, revealing an establishment-outsider dimension invisible when bills serve merely as uninterpretable scaling instruments.

We establish Euclidean distance as the appropriate measurement framework for legislative voting analysis when researchers seek to identify coalitions, measure party cohesion, or compare polarization across dimensions—applications that require but cannot be justified under non-metric utility functions.

The distance-based formulation provides three fundamental advantages for roll-call voting analysis beyond simply restoring metric properties.

The first advantage is enhanced dimensional efficiency. As demonstrated by Nakis et al. (2025), three canonical bipartite embedding operators exist: (i) a low-rank dot-product (LPCA) model $R_{\text{LPCA}}(\mathbf{X}, \mathbf{Y}) = \mathbf{XY}^\top$; (ii) an eigen/inner-product model with additive bias $R_{\text{EIG}}(\mathbf{X}, \mathbf{Y}, \beta) = \beta \mathbf{1} \mathbf{1}^\top + \mathbf{XY}^\top$; and (iii) a Euclidean distance model $R_{L_2}(\mathbf{X}, \mathbf{Y}, \beta)$ with entries $R_{L_2}(i, j) = \beta - \|\mathbf{x}_i - \mathbf{y}_j\|_2$. Let D_{LPCA} , D_{EIG} , and D_{L_2} denote the minimal latent dimensions required to represent a given relation exactly under each operator. Relative to the PCA baseline, Nakis et al. (2025) establish tight bounds $D_{\text{LPCA}} - 1 \leq D_{\text{EIG}} \leq D_{\text{LPCA}}$ and $D_{\text{LPCA}} - 2 \leq D_{L_2} \leq D_{\text{LPCA}}$. Adding a bias term can reduce dimensionality by at most one, whereas the distance formulation can reduce it by as many as two. In homophilous settings—precisely those characteristic of legislative voting—the L_2 geometry achieves the same structural fit with strictly lower or equal dimensionality than inner-product approaches, yielding more parsimonious and interpretable embeddings.

The second advantage is balanced influence across units. Distance-based models rely solely on interpoint distances rather than on the magnitudes of latent vectors. Because only relative positions matter, no legislator or bill can gain disproportionate leverage through unusually large norms. This guards against domination by influential outliers—procedural “hubs” or omnibus measures that touch many issues—and yields more even contribution to estimation across both modes of the bipartite roll-call matrix, producing representations that reflect proximity patterns rather than scale artifacts.

The third advantage is metric coherence through triangle inequality enforcement. Euclidean distance inherently satisfies reflexivity, symmetry, and triangle inequality, imposing global consistency requirements on local similarity relationships. This metric structure eliminates paradoxical spatial configurations where legislator A appears close to B , B close to C , yet A remains distant from C . The resulting mathematical coherence stabilizes coalition detection algorithms, preserves shortest-path interpretability, and enables neighborhood-based analytical summaries that conventional non-metric methods cannot support.

These combined properties establish Euclidean LSIRM as particularly well suited for bipartite roll-call analysis when the goal extends beyond ordinal scaling. The bipartite network framework, by treating legislators and bills symmetrically in a shared metric space, enables bill locations to serve as interpretive anchors that define dimensional meaning and clarify which issues generate cross-cutting cleavages. This restores consistency between spatial voting theory, which assumes proximity preferences over metric distances, and empirical estimation, which should produce estimates that support distance-based inference.

Three extensions merit development. First, dynamic specifications tracking coalition reconfiguration across sessions could model legislator positions as evolving while maintaining metric structure within periods, enabling analysis of how factional boundaries shift over time. Second, incorporating bill metadata (i.e., texts, issue codes, sponsors) through hierarchical priors could sharpen interpretation by partially pooling bill locations within policy domains while permitting cross-issue variation. Third, applications to multiparty systems could further exploit Euclidean distance’s dimensional efficiency, potentially enabling more parsimonious representations of complex coalition structures in fragmented legislatures where conventional methods struggle with high dimensionality. Each extension would require addressing identification and missing data issues particular to its context, but the fundamental advantages—dimensional efficiency, balanced influence, and metric coherence—apply broadly across institutional settings where researchers seek to identify voting coalitions rather than merely scale legislators ordinally.

Acknowledgments The authors thank the editor, associate editor, and reviewers for their constructive comments. Co-correspondence should be addressed to Jonghee Park, Department of Political Science and International Relations, Seoul National University, Seoul, Republic of Korea, E-mail:

jongheepark@snu.ac.kr, and Ick Hoon Jin, Department of Applied Statistics, Department of Statistics and Data Science, Yonsei University, Seoul, Republic of Korea. E-mail: jjin@yonsei.ac.kr.

Funding Statement This work was partially supported by the National Research Foundation of Korea [grant number NRF-2021S1A3A2A03088949, RS-2023-00217705, RS-2024-00333701; Basic Science Research Program awarded to IHJ].

Competing Interests None.

Data Availability Statement Replication data and code can be found in Harvard Dataverse: \url{https://doi.org/10.1111/pan.12504}.

Ethical Standards The research meets all ethical guidelines, including adherence to the legal requirements of the study country.

Author Contributions Conceptualization: S.L.; I.K.; J.H.P.; I.H.J. Methodology: I.H.J.; J.H.P.; S.L. Software: S.L. Validation: S.L. Formal analysis: S.L. Data curation: S.L.; I.K. Visualization: S.L. Writing—original draft: S.L.; J.H.P. Writing—review & editing: S.L.; I.K.; J.H.P.; I.H.J. Supervision: J.H.P.; I.H.J. All authors approved the final submitted draft.

Supplementary Material The supplementary material provides full simulation specifications and extended results for all scenarios, as well as complete MCMC convergence diagnostics and additional analyses of bill positions in the 118th U.S. House.

Notes

References

Airoldi, Edoardo M., David M. Blei, Stephen E. Fienberg, and Eric P. Xing. 2008. Mixed membership stochastic blockmodels. *Journal of Machine Learning Research* 9 (65): 1981–2014. issn: 1533-7928, accessed September 1, 2025. <http://jmlr.org/papers/v9/airoldi08a.html>.

Barberá, Pablo. 2015. Birds of the same feather tweet together: bayesian ideal point estimation using twitter data. *Political Analysis* 23 (1): 76–91.

Binding, Garret, and Lukas F Stoetzer. 2023. Non-separable preferences in the statistical analysis of roll call votes. *Political Analysis* 31 (3): 352–365.

Clarke, Andrew J. 2020. Party sub-brands and american party factions. *American Journal of Political Science* 64 (3): 452–470. <https://doi.org/https://doi.org/10.1111/ajps.12504>. eprint: <https://onlinelibrary.wiley.com/doi/pdf/10.1111/ajps.12504>. <https://onlinelibrary.wiley.com/doi/abs/10.1111/ajps.12504>.

Clinton, Joshua, Simon Jackman, and Douglas Rivers. 2004. The statistical analysis of roll call data. *American Political Science Review* 98 (2): 355–370.

Daudin, J.-J., F. Picard, and S. Robin. 2008. A mixture model for random graphs. *Statistics and Computing* 18 (2): 173–183. issn: 1573-1375. <https://doi.org/10.1007/s11222-007-9046-7>. <https://doi.org/10.1007/s11222-007-9046-7>.

Davis, Otto A, Melvin J Hinich, and Peter C Ordeshook. 1970. An expository development of a mathematical model of the electoral process. *American Political Science Review* 64 (2): 426–448.

Downs, Anthony. 1957. *An economic theory of democracy*. Harper & Row.

Duck-Mayr, JBrandon, and Jacob Montgomery. 2023a. Ends against the middle: measuring latent traits when opposites respond the same way for antithetical reasons. *Political Analysis* 31 (4): 606–625. <https://doi.org/10.1017/pan.2022.33>.

—. 2023b. Ends against the middle: measuring latent traits when opposites respond the same way for antithetical reasons. *Political Analysis* 31 (4): 606–625. <https://doi.org/10.1017/pan.2022.33>.

Fortunato, Santo. 2010. Community detection in graphs. *Physics Reports* 486 (3): 75–174.

Handcock, M. S., A. E. Raftery, and J. M. Tantrum. 2007. Model-based clustering for social network. *Journal of the Royal Statistical Society, Series A* 170:301–354.

Harbridge-Yong, Laurel, Craig Volden, and Alan Wiseman. 2023. The bipartisan path to effective lawmaking. *The Journal of Politics* 85:1048–1063. <https://doi.org/10.1086/723805>.

Hoff, P., A. Raftery, and M. S. Handcock. 2002. Latent space approaches to social network analysis. *Journal of the American Statistical Association* 97 (460): 1090–1098.

Hoff, Peter. 2007. Modeling homophily and stochastic equivalence in symmetric relational data. *Advances in neural information processing systems* 20.

———. 2009. Multiplicative latent factor models for description and prediction of social networks [in en]. *Comput Math Organ Theory* 15 (4): 261–272. issn: 1572-9346, accessed September 1, 2025. <https://doi.org/10.1007/s10588-008-9040-4>.

———. 2021. Additive and multiplicative effects network models. *Statistical Science* 36 (1): pp. 34–50. issn: 08834237, 21688745, accessed September 12, 2025. <https://www.jstor.org/stable/26997946>.

Holland, Paul W., Kathryn Blackmond Laskey, and Samuel Leinhardt. 1983. Stochastic blockmodels: first steps. *Social Networks* 5 (2): 109–137. issn: 0378-8733. [https://doi.org/10.1016/0378-8733\(83\)90021-7](https://doi.org/10.1016/0378-8733(83)90021-7).

Jackman, Simon. 2024. *pscl: classes and methods for R developed in the political science computational laboratory*. R package version 1.5.9. Sydney, Australia: University of Sydney. <https://github.com/atahk/pscl/>.

Jeon, Minjeong, Ick Hoon Jin, Michael Schweinberger, and Samuel Baugh. 2021. Mapping unobserved item-respondent interactions: a latent space item response model with interaction map. *Psychometrika* 86 (2): 378–403.

Karrer, Brian, and M. E. J. Newman. 2011. Stochastic blockmodels and community structure in networks. *Phys. Rev. E* 83 (1): 016107. <https://doi.org/10.1103/PhysRevE.83.016107>.

Kemp, Charles, Joshua B. Tenenbaum, Thomas L. Griffiths, Takeshi Yamada, and Naonori Ueda. 2006. Learning systems of concepts with an infinite relational model. In *Proceedings of the 21st national conference on Artificial intelligence - Volume 1*, 381–388. AAAI'06. Boston, Massachusetts: AAAI Press. ISBN: 978-1-57735-281-5, accessed August 31, 2025.

Kim, In Song, John Londregan, and Marc Ratkovic. 2018. Estimating spatial preferences from votes and text. *Political Analysis* 26 (2): 210–229.

Krivitsky, Pavel N., and Mark S. Handcock. 2008. Fitting position latent cluster models for social networks with latentnet. *Journal of Statistical Software* 24 (5). <https://doi.org/10.18637/jss.v024.i05>.

Lei, Rayleigh, and Abel Rodriguez. 2025. A novel class of unfolding models for binary preference data. *Political Analysis* 33 (1): 32–48.

Lewis, Jeffrey B., Keith Poole, Howard Rosenthal, Adam Boche, Aaron Rudkin, and Luke Sonnet. 2025. *Voterview: congressional roll-call votes database*. Data retrieved from Voterview.com. <https://voterview.com>.

Li, Wu-Jun, Dit-Yan Yeung, and Zhihua Zhang. 2011. Generalized latent factor models for social network analysis. In *Proceedings of the Twenty-Second international joint conference on Artificial Intelligence - Volume Volume Two*, 1705–1710. IJCAI'11. Barcelona, Catalonia, Spain: AAAI Press. ISBN: 978-1-57735-514-4, accessed August 31, 2025.

Lipman, Erin, Scott Moser, and Abel Rodriguez. 2025. Explaining differences in voting patterns across voting domains using hierarchical bayesian models. *Political Analysis*, 1–21.

Lo, Adeline, Santiago Olivella, and Kosuke Imai. 2023. A statistical model of bipartite networks: application to cosponsorship in the united states senate. *arXiv preprint arXiv:2305.05833*.

Marble, William, and Matthew Tyler. 2022. The structure of political choices: distinguishing between constraint and multidimensionality. *Political Analysis* 30 (3): 328–345.

McCarty, Nolan. 2016. In defense of DW-NOMINATE [in en]. *Stud. Am. Pol. Dev.* 30 (2): 172–184. issn: 0898-588X, 1469-8692, accessed August 31, 2025. <https://doi.org/10.1017/S0898588X16000110>.

https://www.cambridge.org/core/product/identifier/S0898588X16000110/type/journal_article.

Miller, Kurt, Michael Jordan, and Thomas Griffiths. 2009. Nonparametric latent feature models for link prediction. In *Advances in Neural Information Processing Systems*, edited by Y. Bengio, D. Schuurmans, J. Lafferty, C. Williams, and A. Culotta, vol. 22. Curran Associates, Inc. https://proceedings.neurips.cc/paper_files/paper/2009/file/437d7d1d97917cd627a34a6a0fb41136-Paper.pdf.

Mørup, Morten, Mikkel N. Schmidt, and Lars Kai Hansen. 2011. Infinite multiple membership relational modeling for complex networks. In *2011 ieee international workshop on machine learning for signal processing*, 1–6. <https://doi.org/10.1109/MLSP.2011.6064546>.

Moser, Scott, Abel Rodríguez, and Chelsea L Lofland. 2021. Multiple ideal points: revealed preferences in different domains. *Political Analysis* 29 (2): 139–166.

Nakis, Nikolaos, Niels Raunkjær Holm, Andreas Lyhne Fiehn, and Morten Mørup. 2025. How low can you go? searching for the intrinsic dimensionality of complex networks using metric node embeddings. *arXiv preprint arXiv:2503.01723*.

Nowicki, Krzysztof, and Tom A. B. Snijders. 2001. Estimation and prediction for stochastic blockstructures. *Journal of the American Statistical Association* 96 (455): 1077–1087. issn: 0162-1459, accessed September 1, 2025. <https://www.jstor.org/stable/2670253>.

Palla, Konstantina, David A. Knowles, and Zoubin Ghahramani. 2012. An infinite latent attribute model for network data. In *Proceedings of the 29th international conference on international conference on machine learning*, 395–402. ICML’12. Edinburgh, Scotland: Omnipress. ISBN: 9781450312851.

Poole, Keith T., and Howard Rosenthal. 2007. *Ideology and congress*. New York: Routledge.

Raftery, A.E., X. Niu, P.D. Hoff, and K.Y. Yeung. 2012. Fast inference for the latent space network model using a case-control approximate likelihood. *Journal of Computational and Graphical Statistics* 21 (4): 909–919.

Schweinberger, M., and Tom A.B. Snijders. 2003. Settings in social networks: a measurement model. *Sociological Methodology* 33:307–341.

Sewell, D. K., and Y. Chen. 2015. Latent space models for dynamic networks. *Journal of the American Statistical Association* 110:1646–1657.

Shin, Sooahn, Johan Lim, and Jong Hee Park. 2024. l_1 -based bayesian ideal point model for multidimensional politics. *Journal of the American Statistical Association* 120 (550): 631–644. <https://doi.org/10.1080/01621459.2024.2425461>. eprint: <https://doi.org/10.1080/01621459.2024.2425461>.

Smith, Anna L, Dena M Asta, and Catherine A Calder. 2019. The geometry of continuous latent space models for network data. *Statistical science: a review journal of the Institute of Mathematical Statistics* 34 (3): 428.

Vu, Duy Q., David R. Hunter, and Michael Schweinberger. 2013. Model-based clustering of large networks. *The Annals of Applied Statistics* 7 (2): 1010–1039. <https://doi.org/10.1214/12-AOAS617>.

Young, Stephen J., and Edward R. Scheinerman. 2007. Random dot product graph models for social networks [in en]. In *Algorithms and Models for the Web-Graph*, edited by Anthony Bonato and Fan R. K. Chung, 138–149. Berlin, Heidelberg: Springer. ISBN: 978-3-540-77004-6. https://doi.org/10.1007/978-3-540-77004-6_11.

Zhou, Mingyuan. 2015. Infinite edge partition models for overlapping community detection and link prediction. In *Artificial intelligence and statistics*, 1135–1143. PMLR.